

Møller Polarimetry With Atomic Hydrogen Targets

Eugene Chudakov and Vladimir Luppov

Abstract—A novel proposal of using polarized atomic hydrogen gas, stored in an ultracold magnetic trap, as the target for electron-beam polarimetry based on Møller scattering is discussed. Such a target of practically 100% polarized electrons could provide a superb systematic accuracy of about 0.5% for beam polarization measurements. Feasibility studies for the CEBAF electron beam have been performed.

Index Terms—Electron beams, helium, hydrogen, Moeller, Møller, polarimetry, polarization.

I. INTRODUCTION

PRECISE electron-beam polarimetry will become increasingly important for the next generation of parity violation experiments. For example, the measurement of the neutron skin of the ^{208}Pb nucleus, proposed at Jefferson Lab [1], requires a 1% polarimetry accuracy for the 850-MeV 50- μA polarized electron beam. Electron-beam polarimetry utilizes QED-calculable polarization-dependent processes. At such energies, two types of polarimeters (Compton and Møller) are widely used. Both types use polarized targets and measure the beam polarization \mathcal{P}_B as $\mathcal{P}_B = A_{\text{obs}}/(\mathcal{P}_T \cdot A)$, where A_{obs} is the observed asymmetry, driven by the beam helicity, \mathcal{P}_T is the target polarization, and A is the analyzing power of the process.

The first type of polarimeter uses Compton scattering of the longitudinally polarized beam electrons on circularly polarized laser light. The light polarization is close to 100% and is relatively easily measurable. The analyzing power depends sharply on the Lab frame energy of the final state photon. Compton polarimetry is accurate enough at beam energies >4 GeV. At Jefferson Lab, the Compton polarimeter of Hall A [2] provides a systematic error of $\sim 1\%$, while 1% statistical error can be achieved in about a 1 h measurement. At lower energies, accurate measurements are more difficult. The analyzing power of Compton scattering A_C depends on the initial electron and photon energies (E_e and k_γ in Lab frame) and, at $E_e < 20$ GeV, the analyzing power A_C is proportional to $k_\gamma E_e$. The maximum energy of the final state photon depends on the initial energies: $k_{\gamma\text{max}} \approx 4k_\gamma(E_e/m_e)^2$, where m_e is the electron's mass. For the beam energy and current discussed, Compton

polarimetry requires a high power light source, typically provided by infrared lasers. For the light wavelength of 1 μm , at $E_e = 850$ MeV, the maximum analyzing power is only $\sim 1\%$, and the maximum photon energy of ~ 13 MeV is uncomfortably low. So far, 1% accurate Compton polarimetry at such energies has not been realized.

The second type of polarimeter uses Møller scattering of the longitudinally polarized beam electrons on longitudinally polarized target electrons, at angles of about 90° in CM. Møller scattering has several advantages over Compton scattering for polarimetry. Its counting rate does not depend on the beam energy. The analyzing power is high (about 80%) and depends neither on the energy, nor does it change substantially in the range of the polarimeter acceptance. Two electrons, with energies $\sim E_e/2$ in the final state, are easily detectable in coincidence, which reduces the background to negligible levels. The disadvantage of Møller polarimetry is associated with polarized electron targets. All Møller polarimeters developed to date utilize magnetized ferromagnetic foils as the polarized electron target (see, for example, [3]–[9]). Such targets provide electron polarization of about 8% (about 2.2 electrons per iron atom are polarized at saturation). The target thickness along the beam should be limited to 0.03–0.3 mm, depending on the beam energy, by electron multiple scattering, bremsstrahlung, double scattering, etc. Since a foil can be easily magnetized in an external magnetic field parallel to its surface, a typical polarimeter uses a foil tilted at about 20° to the beam and magnetized in a field of 10–30 mT, parallel to the beam. The foil polarization has to be measured and is known typically with an accuracy of about 2%–3% relative.

A different approach [9] uses a very strong magnetic field of ~ 4 T along the beam, magnetizing to saturation an iron foil positioned perpendicular to the beam. Because of full saturation, the world data on the properties of pure iron are used, providing a $\sim 0.3\%$ accuracy on the target polarization.

Unfortunately, there are also other systematic errors associated with the ferromagnetic targets. These targets are heated up by the beam and, since heating affects the foil polarization, the beam current must be limited to 2–3 μA . In contrast, the physics experiments often require a much higher current, up to 100 μA . Therefore, the polarization measurements can not run simultaneously with the experiment and have to use a different beam regime. This may be a source of systematic errors, that are difficult to evaluate.

Another source of errors is related to the heavy atoms used for the target. Møller scattering off electrons from the internal atomic shells has a distorted energy-angle correlation of the secondary electrons, compared to scattering off electrons from the external shells. A difference of the polarimeter acceptance for

Manuscript received November 14, 2003. This work was supported by the Southeastern Universities Research Association (SURA), which operates the Thomas Jefferson National Accelerator Facility for the United States Department of Energy under Contract DE-AC05-84ER40150.

E. Chudakov is with Thomas Jefferson National Accelerator Facility, Newport News, VA 23606 USA (e-mail: gen@jlab.org).

V. Luppov was with University of Michigan Spin Physics Center, Ann Arbor, MI 48109 USA. He is now with Janis Research Company, Wilmington, MA 01887 USA (e-mail: vluppov@umich.edu).

Digital Object Identifier 10.1109/TNS.2004.832575

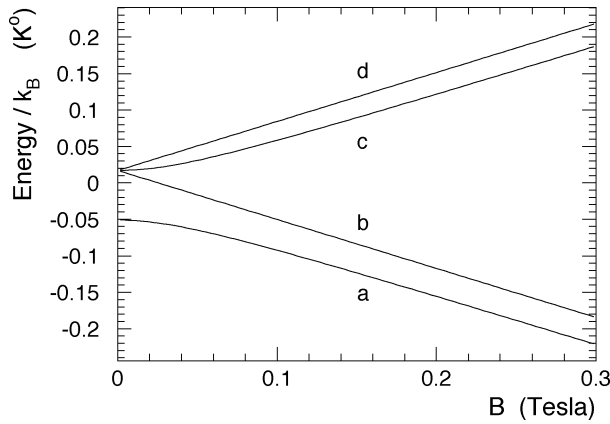


Fig. 1. Splitting of hydrogen levels in a magnetic field. The vertical axis presents the relative energy of the level, divided by the Boltzmann constant k_B . Curves $b-d$ present the spin triplet state of the electron plus proton, while curve a presents the spin singlet state. To resolve the curves on the picture, the plot is limited to low magnetic fields.

these two classes of events is the source of a systematic error (the so-called Levchuk effect [10]), which is typically about 1%. This effect forbids the use of a strong optical collimation of the secondary particles, normally used for background suppression.

In most cases, the background is dominated by electron-nucleus scattering and contains one electron in the final state. This background can be efficiently suppressed by detecting both secondary Møller electrons in coincidence. However, for most of the existing Møller polarimeters, this leads to a dead time of several percent, providing a systematic error hardly much better than 1%. Also, the dead time prevents running at high beam currents, along with target heating described above. It is difficult to use a ferromagnetic target thinner than 4–5 μm ; therefore, the counting rate can be reduced only by reducing the polarimeter acceptance. Unfortunately, this increases the error coming from the Levchuk effect.

With all this in mind it seems very attractive to use atomic hydrogen gas, held in an ultracold magnetic trap [11], as the source of 100% polarized electrons. Møller polarimetry with such a target would be free of the accuracy limitations discussed above. Here, a feasibility study of such an option is presented. The main questions addressed are as follows:

- Target construction and parameters;
- Target density and polarimeter statistical accuracy;
- The effect of the beam on the target parameters.

II. POLARIZED ATOMIC HYDROGEN TARGET

A. Hydrogen Atom in Magnetic Field

The magnetic field B_S and the hyperfine interaction split the ground state of hydrogen into four states with different energies as shown in Fig. 1. The low energy states are $|a\rangle = |\downarrow \uparrow\rangle \cdot \cos\theta - |\uparrow \downarrow\rangle \cdot \sin\theta$ and $|b\rangle = |\downarrow \downarrow\rangle$, where the first and second (crossed) arrows in the brackets indicate the electron and proton spin projections on the magnetic field direction. As far as the electron spin is concerned, state $|b\rangle$ is pure, while state $|a\rangle$ is a superposition. The mixing angle θ depends on the magnetic field B_S and temperature T : $\tan 2\theta \approx 0.05 \text{ T}/B_S$. At $B_S = 8 \text{ T}$ and $T = 0.3 \text{ K}$ the mixing factor is small: $\sin\theta \approx 0.003$. State

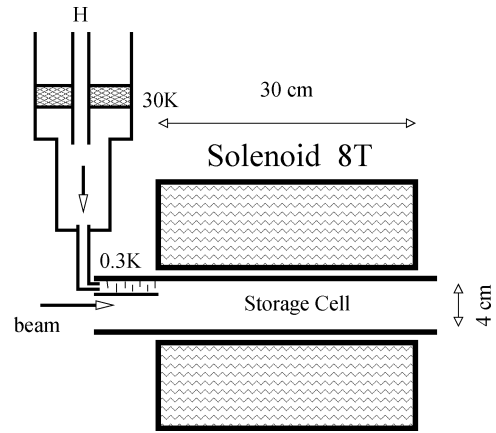


Fig. 2. A sketch of the storage cell.

$|b\rangle$ is 100% polarized. State $|a\rangle$ is polarized in the same direction as $|b\rangle$ and its polarization differs from unity by $\sim 10^{-5}$.

B. Storage Cell

In a magnetic field gradient, a force $-\nabla(\vec{\mu}_H \vec{B})$, where μ_H is the atom's magnetic moment, separates the lower and the higher energy states. The lower energy states are pulled into the stronger field, while the higher energy states are repelled from the stronger field. The 0.3-K cylindrical storage cell, made usually of pure copper, is located in the bore of a superconducting $\sim 8 \text{ T}$ solenoid. The polarized hydrogen, consisting of the low energy states, is confined along the cell axis by the magnetic field gradient, and laterally by the wall of the cell (Fig. 2).

At the point of statistical equilibrium, the state population p follows the Boltzmann distribution

$$p \propto \exp\left(\frac{\mu_e B}{kT}\right) \quad (1)$$

where μ_e is the electron's magnetic moment ($\mu_H \approx \mu_e$) and $k = k_B$ is the Boltzmann constant. The cell is mainly populated with states $|a\rangle$ and $|b\rangle$, with an admixture of states $|c\rangle$ and $|d\rangle$ of $\exp(-2\mu_e B/kT) \approx 3 \cdot 10^{-16}$. In the absence of other processes, states $|a\rangle$ and $|b\rangle$ are populated nearly equally. The gas is practically 100% polarized, a small ($\sim 10^{-5}$) oppositely polarized contribution comes from the $|\uparrow \uparrow\rangle$ component of state $|a\rangle$.

The atomic hydrogen density is limited mainly by the process of recombination into H_2 molecules (releasing $\sim 4.5 \text{ eV}$). The recombination rate is higher at lower temperatures. In gas, recombination by collisions of two atoms is kinematically forbidden but it is allowed in collisions of three atoms. On the walls, which play the role of a third body, there is no kinematic limitation for two atom recombination. At moderate gas densities only the surface recombination matters. In case of polarized atoms, the cross section for recombination is strongly suppressed, because two hydrogen atoms in the triplet electron spin state have no bound states. This fact leads to the possibility of reaching relatively high gas densities for polarized atoms in the traps.

A way to reduce the surface recombination on the walls of the storage cell is coating them with a thin film ($\sim 50 \text{ nm}$) of

superfluid ^4He . The helium film has a very small sticking coefficient¹ for hydrogen atoms.² In contrast, hydrogen molecules in thermal equilibrium with the film are absorbed after a few collisions and are frozen in clusters on the metal surface of the trap [12].

The higher energy states are repelled from the storage cell by the magnetic field gradient and leave the cell. Outside of the helium-covered cell, the atoms promptly recombine on surfaces into hydrogen molecules which are either pumped away or are frozen on the walls. Some of the higher energy states recombine within the cell and the molecules eventually are either frozen on the helium-coated wall, or leave the cell by diffusion.

The cell is filled with atomic hydrogen from an RF dissociator. Hydrogen, at 80 K, passes through a Teflon³ pipe to a nozzle, which is kept at ~ 30 K. From the nozzle hydrogen enters into a system of helium-coated baffles, where it is cooled down to ~ 0.3 K. At 30 K and above, the recombination is suppressed because of the high temperature, while at 0.3 K it is suppressed by helium coating. In the input flow, the atoms and molecules are mixed in comparable amounts, but most of the molecules are frozen out in the baffles and do not enter the cell.

The gas arrives at the region of a strong field gradient, which separates very efficiently the lower and higher atomic energy states, therefore, a constant feeding of the cell does not affect the average electron polarization.

This technique was first successfully applied in 1980 [13], and later a density⁴ as high as $3 \cdot 10^{17}$ atoms/cm³ was achieved [11] in a small volume. It was then proposed to use the electron-spin-polarized atomic hydrogen in proton-spin-polarized sources and targets [14]–[17], by extracting the gas from the storage cell and creating a jet of polarized atoms. So far, the storage cell itself has not been put in a high-intensity particle beam.

For the project being discussed, a normal storage cell design can be used, with the beam passing along the solenoid axis (Fig. 2). The double walls of the cylindrical copper cell form a dilution refrigerator mixing chamber. The cell is connected to the beam pipe with no separating windows. The tentative cell parameters are (similar to a working cell [17]):

- Solenoid maximum field $B_S = 8$ T.⁵
- Solenoid length $L_S = 30$ cm.
- Cell internal radius $r_o = 2$ cm.
- Cell length $L_C = 35$ cm.
- Temperature $T = 0.3$ K.

The gas density dependence on the coordinate z along the solenoid axis follows (1) and is shown in Fig. 3. The effective

¹The sticking coefficient defines the atom's adsorption probability per a collision with a surface.

²The recombination rates are discussed quantitatively in Section II-D.

³Teflon has a relatively small sticking coefficient for hydrogen atoms.

⁴This parameter is called concentration, but we will use the word density in the text, since the mass of the gas is not important here.

⁵We used the parameters of a standard solenoid magnet manufactured by AMI (American Magnetics, Inc.). This magnet has a 10^{-5} uniformity inside the 1 cm diameter central sphere. Such a magnet has been successfully used in a similar atomic hydrogen storage cell [17]. We used the calculated field on the solenoid axis, provided by AMI and assumed that the field is uniform across the cell cross section. The latter assumption is good enough for these studies of possible impacts of the beam on the storage cell, since these impacts are most important in the region close to the beam.

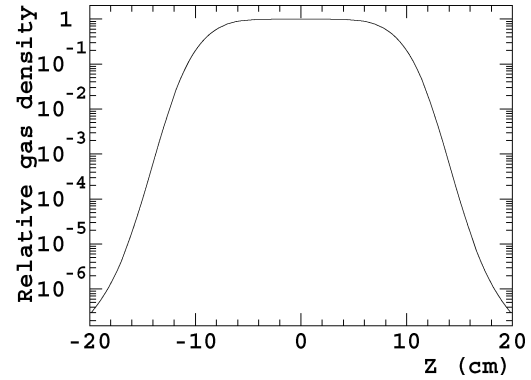


Fig. 3. The relative gas distribution along the solenoid axis.

length of such a target is about 20 cm. The solenoid field has to be reasonably uniform in this volume of the cell, to avoid regions where the gas density is higher than on the axis. In such regions, the recombination speed is increased without increasing the luminosity. The field in the volume should not exceed the field at the solenoid center by more than $\sim 2 \cdot 10^{-3}$ (a $\sim 4\%$ increase in the density).

For the guideline, we will consider a gas density of $3 \cdot 10^{15}$ cm⁻³, obtained experimentally [18], for a similar design.

C. Gas Properties

Important parameters of the target gas are the diffusion speed and heat conductance. At 300 mK, the rms speed is $\bar{v} = \sqrt{8kT/\pi m} = 80$ m/s, where m is the atom's mass. The number of collisions per second depends on the atomic scattering cross section σ ([19]): $(dn_{col}/dt) = \sigma \cdot 4n\sqrt{kT/\pi m}$ where n is the gas density and m is the atomic mass. The mean free path is: $\ell = \bar{v}/(dn_{col}/dt) = (\sigma n\sqrt{2})^{-1}$. There are several calculations of the hydrogen atoms cross section [20]–[24] at low temperatures. For these studies we accepted the value $\sigma = 42.3 \cdot 10^{-16}$ cm² [22], ignoring the difference between the spin triplet and singlet cross sections. The effective atom diameter is $d = \sqrt{\sigma/\pi} = 3.69 \cdot 10^{-8}$ cm. This would provide $(dn_{col}/dt) \approx 1.4 \cdot 10^5$ sec⁻¹ and $\ell = 0.57$ mm, at 0.3 K and density of $3 \cdot 10^{15}$ cm⁻³.

The average time, τ_d for a “low field seeking” atom to travel to the edge of the cell, assuming its starting point is distributed according to the gas density, is ⁶ $\tau_d \propto (d^2/\sqrt{T})n$, $\tau_d \approx 0.7$ s. This is the cleaning time for an atom with opposite electron spin, should it emerge in the cell and if it does not recombine before. The escape time depends on the initial position of the atom, going from ~ 1 s at $z = 0$ to 0.1 s at $z = 8$ cm. The average wall collision time is about 0.5 ms.

D. Gas Lifetime in the Cell

For the moment, we consider the gas behavior with no beam passing through it. Several processes lead to losses of hydrogen atoms from the cell:

- 1) thermal escape through the magnetic field gradient;
- 2) recombination in the volume of gas;
- 3) recombination on the surface of the cell.

⁶This time was estimated using simulation, taking into account the gas density distribution along z and the repelling force in the magnetic field gradient.

The thermal escape can be characterized by the average escape time τ_{es}

$$\tau_{es} = \tau_d \cdot \exp\left(\frac{\mu_e(B - B_e)}{kT}\right) \quad (2)$$

where τ_d (see Section II-C) is the average time for an atom to drift to the edge of the cell, or to the area of strong field gradient, while B and B_e are the magnetic fields at the center and at the edge of the cell. We selected $B_e/B = 0.3$.

The volume recombination can be neglected up to densities of $\sim 10^{17} \text{ cm}^{-3}$ [11].

The surface recombination cross section can be characterized by a factor [11]

$$\mathcal{K}_s^{\text{eff}} = 5 \cdot 10^{-8} \frac{A}{V} \Lambda^2 \exp\left(\frac{2\varepsilon_a}{kT}\right) \frac{\sqrt{T}}{B^2} \quad (3)$$

where A is the storage surface area, V is the storage volume, $\Lambda = \hbar\sqrt{2\pi/kTm} \approx 1.74 \cdot 10^{-7}/\sqrt{T}$ is the thermal de Broglie wavelength and $\varepsilon_a \approx 1 \text{ K}$ is the H absorption energy on the He surface. The sizes are measured in cm.

One should note that (3) presents a simplified model, ignoring the difference between states $|a\rangle$ and $|b\rangle$. In reality, a small admixture of the opposite electron polarization in state $|a\rangle$ considerably increases its recombination rate with both $|a\rangle$ and $|b\rangle$ atoms. Therefore, as a result, state $|a\rangle$ is depleted faster than $|b\rangle$. If no fast relaxation between $|a\rangle$ and $|b\rangle$ happens (it may happen on magnetic impurities on the cell surface), the population ratio $|a\rangle/|b\rangle$ drops with time and the recombination rate slows down.

To keep the gas density constant, the losses have to be compensated by constantly feeding the cell with atomic hydrogen at a very moderate rate of $\Phi \sim 1 - 10 \cdot 10^{15}$ atoms/s. The balance condition is

$$\frac{\Phi}{V} = \mathcal{K}_s^{\text{eff}} n^2 + n \frac{1}{\tau_{es}} \quad (4)$$

where n is the gas density. The parameter τ_{es} [see (2)] depends on the density. These equations help to specify the optimal cell parameters:⁷

$$B_S > 7 \text{ T}, \quad T \sim 0.3 \text{ K}. \quad (5)$$

For $B_S = 8 \text{ T}$, $T = 0.3 \text{ K}$, and $\Phi = 1 \cdot 10^{15} \text{ s}^{-1}$, the calculated density is $n \approx 7 \cdot 10^{15} \text{ cm}^{-3}$.⁸ The gas is mostly lost to recombination. The average lifetime of an atom in the cell is $nV/\Phi \sim 1 \text{ h}$. Comparing this lifetime with the time to travel between the cell edges of $\sim 1 \text{ s}$ we see that the gas has time to populate the different field areas according to (1).

One should note that at very low densities the losses are dominated by the thermal escape through the field gradient, with an average lifetime of $\sim 600 \text{ s}$.

E. Unpolarized Contamination

The most important sources of unpolarized contamination in the target gas in absence of beam have been identified:

⁷It should be pointed out that the temperature should not exceed $\sim 0.4 \text{ K}$, because of a high helium gas pressure beyond this.

⁸The same calculation made for 0.2 K predicts a density of $1.3 \cdot 10^{15} \text{ cm}^{-3}$. This can be compared with the measurement [18] of $3 \cdot 10^{15} \text{ cm}^{-3}$.

- 1) hydrogen molecules: $\sim 10^{-5}$;
- 2) high energy atomic states $|c\rangle$ and $|d\rangle$: $\sim 10^{-5}$;
- 3) excited atomic states $< 10^{-10}$;
- 4) other gasses, like helium and the residual gas in the cell: $\sim 10^{-3}$.

The contributions 1)–3) are present when the cell is filled with hydrogen. They are difficult to measure directly and we have to rely on calculations. Nevertheless, the behavior of such storage cells has been extensively studied and is well understood [11]. The general parameters, like the gas lifetime, or the gas density are predicted with an accuracy better than a factor of 3. The estimates 1)–3) are about 100 times below the level of contamination of about 0.1% which may become important for polarimetry. In contrast, the contribution 4) can be easily measured with beam by taking an empty target measurement. Atomic hydrogen can be completely removed from the cell by heating a small bolometer inside the cell, which would remove the helium coating on this element, and catalyze a fast recombination of hydrogen on its surface. However, it is important to keep this contamination below several percent in order to reduce the systematic error associated with the background subtraction.

III. BEAM IMPACT ON STORAGE CELL

We have considered various impacts the $\mathcal{I}_b = 100 \mu\text{A}$ CEBAF beam can inflict on the storage cell. The beam consists of short bunches with $\tau = \sigma_T \approx 0.5 \text{ ps}$ at a $\mathcal{F} = 499 \text{ MHz}$ repetition rate. The beam spot has a size of about $\sigma_X \approx \sigma_Y \sim 0.1 \text{ mm}$. The most important depolarization effects we found are:

- a) gas depolarization by the RF electromagnetic radiation of the beam: $\sim 3 \cdot 10^{-5}$;
- b) contamination from free electrons and ions: $\sim 10^{-5}$;
- c) gas excitation and depolarization by the ionization losses: $\sim 10^{-5}$;
- d) gas heating by ionization losses.

A. Beam RF Generated Depolarization

The electromagnetic field of the beam has a circular magnetic field component $B(r, t)$, which couples to the $|a\rangle \rightarrow |d\rangle$ and $|b\rangle \rightarrow |c\rangle$ transitions. The transition frequency depends on the value of the local magnetic field in the solenoid and for the bulk of the gas ranges from 215 to 225 GHz. The spectral density function of the beam magnetic field can be expressed in a Fourier series as $B(r, t) = \sum_{n=-\infty}^{\infty} \hat{B}_n(r) \cdot e^{i\omega_n t}$, and

$$\hat{B}_n(r) \approx B(r) \frac{\omega_0}{\sqrt{2\pi}} \cdot \exp\left(-\frac{\omega_0^2 n^2 \tau^2}{2}\right) \quad (6)$$

where $\omega_0 = 2\pi\mathcal{F}$. The resonance lines of the spectrum populate densely the transition range (see Fig. 4). The induced transition rate depends on the gas density at a given transition frequency $dN/d\omega_{ad}$

$$N \frac{dV_{a \rightarrow d}}{dt} = \sum_{n=1}^{\infty} \frac{dN}{d\omega_{ad}} \Big|_{\omega_n} \left(\frac{\mu_e \omega_0 B(r)}{\hbar}\right)^2 \cdot \exp(-\omega_0^2 n^2 \tau^2) \quad (7)$$

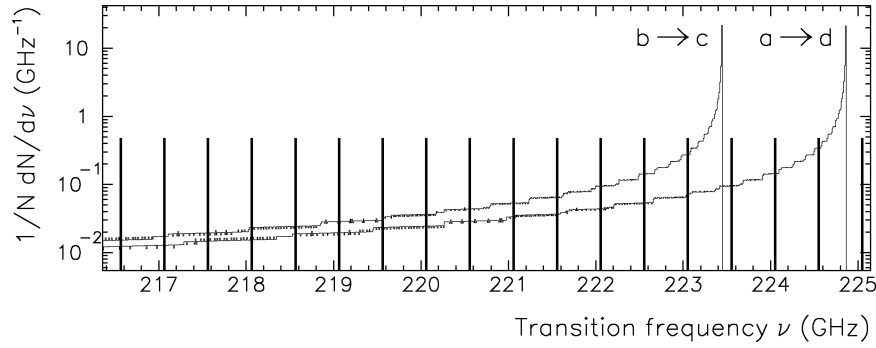


Fig. 4. Simulated spectra of the transitions on the axis of the hydrogen trap with the maximum field of 8.0 T. The density of atoms depends on the field as $\exp(-\mu_e B/kT)$. The two curves show $(1/N)dN/d\nu_{ad}$ and $(1/N)dN/d\nu_{bc}$ —the relative number of atoms which can undergo $|a\rangle \rightarrow |d\rangle$ and $|b\rangle \rightarrow |c\rangle$ transitions at the given frequency, per one GHz. The resonant structure of the spectral function of the beam-induced electromagnetic field is shown as a set of vertical bars, 499 MHz apart.

where the beam-generated magnetic field is expressed in SI

$$B(r) = \frac{\mathcal{I}_b}{\omega_o \epsilon_o c \sqrt{2\pi} \sigma_X} \cdot \left(1 - \exp\left(-\frac{r^2}{2\sigma_X^2}\right)\right) \frac{1}{r}. \quad (8)$$

Provided that the field of the solenoid is fine tuned to avoid the transition resonances for the bulk of the gas in the cell (see Fig. 4), the depolarization described has the following features:

- the average rate of each of the two transitions is about $0.5 \cdot 10^{-4}$ of the target density per second;
- at the center around the beam, the full transition rate is about 6% of the density per second.

To estimate the average contamination we take into account that each resonance line presented in Fig. 4 corresponds to a certain value of the solenoid field and, therefore, affects the gas at a certain z . The resonance lines' concentration is higher in the field gradient area than at the center $z = 0$. On the other hand, the “escape time” depends on the atom's original location and drops from the center of the cell to the edge (see Section II-C). The average depolarization in the beam area will be reduced to about $\sim 0.3 \cdot 10^{-4}$ by the lateral gas diffusion and by the escape of the “low field seeking” atoms from the storage cell.

To study experimentally the depolarization effect discussed, one can tune the solenoid magnetic field to overlap a resonance line with the transition frequency of the gas at the cell center. This would increase the transition rate by a factor of ~ 70 .

The beam may induce electromagnetic waves in the storage cell. The lowest resonant frequency for a long pipe of the radius r_o is [25]: $f \approx 1.84 \cdot c/(2\pi r_o) = 4.4$ GHz, which is about 10 times higher than the beam repetition frequency of 499 MHz, but much lower than the transition frequency of ~ 220 GHz. The impact of such waves on the stored gas is negligible in comparison with the impact discussed earlier.

B. Contamination by Free Electrons and Ions

The beam would ionize per second about 20% of the atoms in the cylinder around the beam spot. The charged particles would not escape the beam area due to diffusion, as the neutral atoms would do, but will follow the magnetic field lines, parallel to the beam. An elegant way to remove them is to apply a relatively weak ~ 1 V/cm electric field perpendicular to the beam. The charged particles will drift at a speed of $v = \vec{E} \times \vec{B}/B^2 \sim 12$ m/s perpendicular to the

beam and leave the beam area in about 20 μ s. This will reduce the average contamination to a 10^{-5} level.

C. Depolarization by Electron Collisions

The beam can excite the atoms. The full energy released by the beam is about $4 \cdot 10^{-4}$ eV \cdot s $^{-1}$ per atom in the target. This is a small value in comparison with the 2P-1S transition energy of ~ 10 eV. If 50% of the energy goes to this excitation, the excited atoms would be produced at a rate of $2 \cdot 10^{-5}$ s $^{-1}$. The P-states have lifetimes of about 1 ns, which reduces the potential contamination to a $\sim 10^{-12}$ level. Eventually, all excited atoms decay to lower S-states. Some S-states have long lifetimes, but in the magnetic trap they are polarized in the same way as the ground 1S state, therefore amounting to a contamination at a $\tau_d \cdot 1 \cdot 10^{-5} \approx 10^{-5}$ level.

The spin-flip transition requires much less energy than the 2P-1S one. We calculated the rate of $|a\rangle \rightarrow |d\rangle$ transitions caused by individual electrons passing close to the atom, in the same way as it was calculated for the bunches in Section III-A. Since the effect is proportional to the square of the electric charge of the beam particle, one may expect that single electrons have less effect than the beam bunch. Indeed, the conclusion is that this rate is negligible.

D. Gas Heating by Beam Ionization

In gaseous hydrogen, a beam particle releases on average 6.3 MeV/(g/cm 2) by ionization. In the target considered, of thickness $\sim 6 \cdot 10^{16}$ atoms/cm 2 , the average loss is 0.6 eV per beam particle. A part of this energy goes to δ -electrons which may leave the cell, spiraling in the magnetic field, if their energy is large enough. A reasonable cutoff for the δ -electron kinetic energy is $T_1 \sim 1$ keV. At this energy, the δ -electron would lose about 100 eV in the target due to ionization losses and carry away the rest of its energy. For the maximum energy we selected $T_2 \sim 0.2T_{\max} = 0.2E_{\text{beam}}$. Then, the full energy carried away by δ -electrons knocked out by one beam particle would be [26]: $E \approx 1.8$ MeV/(g/cm 2). The energy absorbed in the target is $\alpha = 4.5$ MeV/(g/cm 2) from one beam particle. The full energy absorbed per unit length of the target per second is

$$J = \alpha \cdot \frac{\mathcal{I}_b}{q_e} \frac{n}{N_A} \quad (9)$$

where N_A is the Avogadro number and n is the gas density.

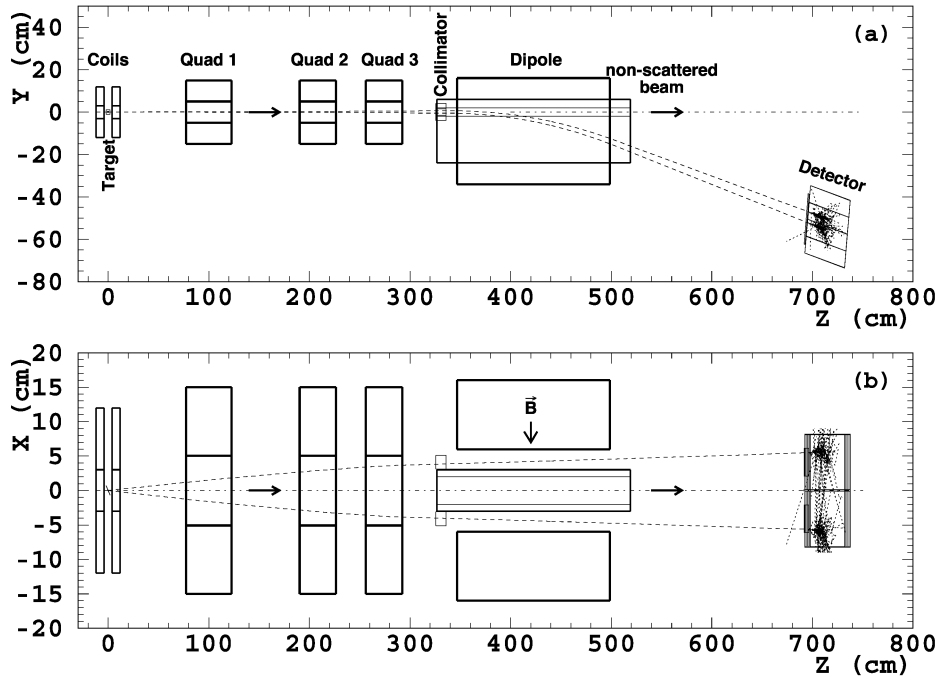


Fig. 5. Layout of the existing Hall A Møller polarimeter. The spectrometer consists of 3 quadrupole magnets and a dipole magnet. The existing target (at $Z = 0$ cm) can be replaced by the atomic hydrogen storage cell (see Fig. 2). The whole cell setup, used in [17], including the magnet and the cryostat, would fit into the space. Thermal screens must be installed in the 10 cm diameter beam pipe in order to reduce the radiation heat load on the cell. The screens should have holes at the center to let the beam pass.

The heat conductance in gas is $\chi = (4k/3\sigma)\sqrt{kT/\pi m}$. Let us assume that the beam profile is flat within a radius r_b , which is a good model if the beam is smeared out by a fast raster. In the absence of the fast raster, this assumption is an approximation. Then, solving the heat flow equation for a very long tube, assuming a fixed temperature T_0 on the tube wall at r_o we obtain

$$\begin{aligned} \Delta T(r) &= T(r) - T_0 = \frac{J}{2\pi\chi} \ln \frac{r_o}{r} \quad r > r_b \\ \Delta T(r) &= T(r) - T_0 \\ &= \frac{J}{2\pi\chi} \left[\ln \frac{r_o}{r_b} + \frac{1}{2} \left(1 - \frac{r^2}{r_b^2} \right) \right] \quad r < r_b. \end{aligned} \quad (10)$$

The temperature increase reaches a maximum at the beam center

$$\Delta T(r) = \alpha \cdot \frac{\mathcal{I}_b}{q_e} \frac{n}{NA} \frac{3\sigma}{8k\pi\sqrt{\frac{kT}{\pi m}}} \left[\ln \frac{r_o}{r_b} + \frac{1}{2} \right] \quad (11)$$

and is proportional to the gas density. For $\mathcal{I}_b = 100 \mu\text{A}$, $n = 3 \cdot 10^{15} \text{ cm}^{-3}$, $\sigma = \pi d^2$, where $d = 3.7 \cdot 10^{-8} \text{ cm}$, and $T = 0.3 \text{ K}$ we get

$$\Delta T(0) = 0.030 \text{ K} \cdot \left[\ln \frac{r_o}{r_b} + \frac{1}{2} \right]. \quad (12)$$

Gas convection was neglected. For the 0.2-mm-diameter beam, the temperature rise at the beam center is about 0.17 K. Fast rastering of the beam to a 4-mm diameter will reduce the rise to about 0.08 K. No serious implication of such a heating is foreseen. The recombination rate and the helium gas pressure depend only on the temperature on the cell walls, which stays at 0.3 K. The mean polarization should not be affected in a noticeable way, since the population of oppositely polarized

states in the equilibrium would go from $\sim 10^{-16}$ to $\sim 10^{-10}$. Due to the Knudsen rule [27], $n \cdot \sqrt{T} = \text{const}$, the gas density at the center will drop by $\sim 20\%$. This change is not very important.

IV. APPLICATION OF THE ATOMIC TARGET TO MØLLER POLARIMETRY

This feasibility study was done for the possible application of the target discussed to the existing Møller polarimeter in Hall A at JLab [8] (see Fig. 5). The results are, however, more generic and are largely applicable to other facilities with “continuous” electron beams.

A. Polarimeter Parameters

1) *Target Density and Statistical Accuracy:* The beam polarization at JLab is normally about 80%, at beam currents below $100 \mu\text{A}$. The Hall A polarimeter acceptance will not be affected significantly by the strong solenoid field in the target region. An atomic hydrogen target 10 cm long⁹ with a density of $3 \cdot 10^{15} \text{ electrons/cm}^3$ provides $3 \cdot 10^{16} \text{ electrons/cm}^2$ thickness. The maximum beam current allowed by the accelerator can be used with this target. We assume here an easily available current of $30 \mu\text{A}$, though currents over $100 \mu\text{A}$ have been delivered. The time needed to achieve a 1% statistical accuracy, estimated by scaling the parameters of the existing polarimeter, would be ≈ 30 min. This is an acceptable time, in particular if the measurements are done in parallel with the main experiment.

⁹The effective target length depends on the beam energy, because of the polarimeter acceptance. At the lowest energy considered—0.850 GeV, the effective length is about 10 cm, while at 5 GeV it is about 20 cm.

2) *Polarimetry Systematic Error:* There is no obvious way to measure directly the polarization of the hydrogen atoms in the beam area. The contamination from the residual gas is measurable. The rest relies on calculations. All calculations show that the polarization is nearly 100%, with a possible contamination of <0.01%, coming from several contributions. The impact of the most important of these contributions can be studied, at least their upper limits, by deliberately increasing the effect. For example, the beam RF induced transitions can be increased by a factor of ~ 70 , by fine tuning of the solenoid magnetic field. The contribution from the charged particles in the beam area can be varied by a factor up to $\sim 10^4$, by changing the cleaning electric field. Also, the contributions discussed depend on the gas density and the beam current. Making the gas lifetime measurements, as well as polarization measurements, under different conditions, such as the density, temperature and beam current would help to establish an upper limit for the target depolarization.

The systematic errors, associated with the present Hall A polarimeter, when added in quadrature give a total systematic error of about 3% [8]. Scaling these errors to the hydrogen target option leaves only those:

- average analyzing power 0.3%;
- background 0.1%.

At this level of accuracy, some other errors, neglected before, may become significant and more work has to be done to identify them. Still, a 0.5% error seems achievable and a 1% error certain.

V. CONCLUSION

The considerations above show that a stored, longitudinally electron-spin-polarized atomic hydrogen can be used as a pure, 100% electron polarized gas target. A thickness of at least $6 \cdot 10^{16}$ electrons/cm² can be reached with a target diameter of 4 cm and a length of 20 cm along the beam. The polarized hydrogen gas should be stable in the presence of a 100 μ A CEBAF beam. A Møller polarimeter, equipped with such a target would provide a superb systematic accuracy of about 0.5%, while providing a 1% statistical accuracy in about 30 min of running at a beam current of 30 μ A.

There are alternative possibilities for precise polarimetry at the energies below 1 GeV.

It has been estimated that the Compton polarimeter [2] of Hall A at JLab, equipped with a powerful green light source could provide a $\sim 1\%$ systematic error. It would need about 15 h to reach a 1% statistical accuracy with a 30- μ A beam.

The only existing Møller polarimeter which can potentially provide a comparable accuracy is the polarimeter [9] of Hall C at JLab. In this polarimeter an iron foil target is perpendicular to the beam. It is saturated in a strong magnetic field of ~ 4 T. The main problem is running at high beam currents. One way to reduce the target heating is to rotate the target. Another way is to reduce the *average* beam current by strobing the beam impact with the target, for example, by moving the beam on the target only for short intervals of time, otherwise sending it bypassing the target. The problem of dead time may become important.

At low beam currents the sources of the two dominant systematic errors of this polarimeter are the target polarization and the Levchuk effect. The polarized atomic hydrogen target should reduce the former error by an order of magnitude, while removing the latter error completely.

A disadvantage of the polarized atomic hydrogen target is a relative complexity of its building and operation, in comparison with the magnetized ferromagnetic foils. It may, however, provide an unprecedented level of accuracy, stimulating a new generation of parity violation experiments.

REFERENCES

- [1] C. J. Horowitz, S. J. Pollock, P. A. Souder, and R. Michaels, *Phys. Rev. C*, vol. 63, pp. 025 501-1–025 501-18, Jan. 2001.
- [2] M. Baylac, E. Burtin, C. Cavata, S. Escoffier, B. Frois, and D. Lhuillier *et al.*, “First electron beam polarization measurements with a Compton polarimeter at Jefferson laboratory,” *Phys. Lett. B*, vol. 539, pp. 8–12, July 2002.
- [3] P. S. Cooper, M. J. Alguard, R. D. Ehrlich, V. W. Hughes, H. Kobayakawa, and J. S. Ladish *et al.*, “Polarized electron-electron scattering at GeV energies,” *Phys. Rev. Lett.*, vol. 34, pp. 1589–1592, June 1975.
- [4] B. Wagner, H. G. Andresen, K. H. Steffens, W. Hartmann, W. Heil, and E. Reichert, “A Møller polarimeter for Cw and pulsed intermediate-energy electron beams,” *Nucl. Instrum. Methods*, vol. A294, pp. 541–548, Sept. 1990.
- [5] J. Arrington, E. J. Beise, B. W. Filippone, T. G. O’Neill, W. R. Dodge, G. W. Dodson, K. A. Dow, and J. D. Zumbro, “A variable energy Møller polarimeter at the MIT bates linear accelerator center,” *Nucl. Instrum. Methods*, vol. A311, pp. 39–48, Jan. 1992.
- [6] K. B. Beard, R. Madey, W. M. Zhang, D. M. Manley, B. D. Anderson, and A. R. Baldwin *et al.*, “Measurement of the polarization of a pulsed electron beam with a Møller polarimeter in the coincidence mode,” *Nucl. Instrum. Methods*, vol. A361, pp. 46–52, July 1995.
- [7] H. R. Band, G. Mitchell, R. Prepost, and T. Wright, “A Møller polarimeter for high energy electron beams,” *Nucl. Instrum. Methods*, vol. A400, pp. 24–33, Nov. 1997.
- [8] A. V. Glamazdin, V. G. Gorbenco, L. G. Levchuk, R. I. Pomatsalyuk, A. L. Rubashkin, and P. V. Sorokin *et al.*, “Electron beam Møller polarimeter at JLAB Hall A,” *Fizika B*, vol. 8, pp. 91–95, 1999.
- [9] M. Hauger, A. Honegger, J. Jourdan, G. Kubon, T. Petitjean, and D. Rohe *et al.*, “A high-precision polarimeter,” *Nucl. Instrum. Methods*, vol. A462, pp. 382–392, Apr. 2001.
- [10] L. G. Levchuk, “The intra-atomic motion of bound electrons as a possible source of a systematic error in electron beam polarization measurements by means of a Møller polarimeter,” *Nucl. Instrum. Methods*, vol. A345, pp. 496–499, July 1994.
- [11] I. F. Silvera and J. T. M. Walraven, “Spin polarized atomic hydrogen,” in *Progress in Low Temperature Physics*. Amsterdam: Elsevier Science B.V., 1986, vol. X, pp. 139–370.
- [12] I. F. Silvera, “Ultimate fate of a gas of atomic hydrogen in a liquid-helium chamber: recombination and burial,” *Phys. Rev. B*, vol. 29, pp. 3899–3904, Apr. 1984.
- [13] I. F. Silvera and J. T. M. Walraven, “Stabilization of atomic hydrogen at low temperature,” *Phys. Rev. Lett.*, vol. 44, pp. 164–168, Jan. 1980.
- [14] T. O. Niinikoski, “Progress in polarized targets,” in *1980 Int. Symp. High Energy Physics With Polarized Beams and Polarized Targets*, Lausanne, 1980, C80-09-25.24 CERN-EP-80-227.
- [15] D. Kleppner and T. J. Greytak, “Spin polarized hydrogen: new possibilities for polarized sources and targets,” in *Proc. High Energy Spin Physics—1982*, Brookhaven, 1982, pp. 546–565.
- [16] M. Mertig, A. V. Levkovich, V. G. Luppov, and Y. K. Pilipenko, “Accumulation of hydrogen atoms in a low temperature storage cell of a polarized hydrogen gas jet source,” in *Proc., High Energy Spin Physics—1990*, vol. 2, Bonn, Germany, 1990, pp. 164–167.
- [17] T. Roser, D. G. Crabb, W. A. Kaufman, R. S. Raymond, J. A. Stewart, B. Vuaridel, and G. R. Court, “Microwave driven extraction of stabilized spin polarized atomic hydrogen,” *Nucl. Instrum. Methods*, vol. A301, pp. 42–46, Feb. 1991.
- [18] M. Mertig, V. G. Luppov, T. Roser, and B. Vuaridel, “Continuous density measurement of atomic hydrogen by means of a bolometer,” *Rev. Sci. Instrum.*, vol. 62, pp. 251–252, Jan. 1991.

- [19] L. D. Landau and E. M. Livshitz, "Statistical physics," in *Theoretical Physics*. Moscow, U.S.S.R.: Nauka, 1979, vol. X.
- [20] M. E. Gersh and R. B. Bernstein, "Calculated total elastic scattering cross sections for H(1S) at collision energies below 1 eV," *Chem. Phys. Lett.*, vol. 4, pp. 221–223, Dec. 1969.
- [21] A. C. Allison and F. J. Smith, "Transport properties of atomic hydrogen," *Atomic Data*, vol. 3, pp. 317–321, Dec. 1971.
- [22] M. D. Miller and L. H. Nosanow, "Possible new quantum systems. II. Properties of the isotopes of spin-aligned hydrogen," *Phys. Rev. B*, vol. 15, pp. 4376–4385, May 1977.
- [23] D. G. Friend and R. D. Etters, "A dilute hard-sphere Bose-gas model calculation of low-density atomic hydrogen gas properties," *J. Low Temp. Phys.*, vol. 39, pp. 409–415, May 1980.
- [24] C. Lhuillier, "Transport properties in a spin polarized gas. III," *J. Physique*, vol. 44, pp. 1–12, Jan. 1983.
- [25] J. D. Jackson, *Classical Electrodynamics*. New York: Wiley, 1975, p. 356.
- [26] K. Hagiwara, K. Hikasa, K. Nakamura, M. Tanabashi, M. Aguilar-Benitez, and C. Amsler *et al.*, "Review of particle physics," *Phys. Rev. D*, vol. 66, p. 010001-197, July 2002.
- [27] M. Knudsen, *Kinetic Theory of Gases*. London, U.K.: Methuen, 1952, pp. 33–34.